Spatiospectral control of spontaneous emission

Seyyed Hossein Asadpour [1,*] Muqaddar Abbas [2,†] Hamid R. Hamedi [3,‡] Julius Ruseckas [4,§]
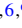Emmanuel Paspalakis [5,‖] and Reza Asgari [1,6,¶]

[1]*School of Physics, Institute for Research in Fundamental Sciences (IPM), Tehran 19395-5531, Iran*
[2]*Ministry of Education Key Laboratory for Nonequilibrium Synthesis and Modulation of Condensed Matter,
Shaanxi Province Key Laboratory of Quantum Information and Quantum Optoelectronic Devices, School of Physics,
Xi'an Jiaotong University, Xi'an 710049, China*
[3]*Institute of Theoretical Physics and Astronomy, Vilnius University, Sauletekio 3, Vilnius 10257, Lithuania*
[4]*Baltic Institute of Advanced Technology, Pilies St. 16-8, LT-01403 Vilnius, Lithuania*
[5]*Materials Science Department, School of Natural Sciences, University of Patras, Patras 265 04, Greece*
[6]*Department of Physics, Zhejiang Normal University, Jinhua, Zhejiang 321004, China*

We propose a scheme aimed at achieving spatiospectral control over spontaneous emission within a four-level atom-light coupling system interacting with optical vortices carrying orbital angular momentum (OAM). The atom comprises a ground level and two excited states coupled with two laser fields, forming a V subsystem where the upper states exclusively decay to a common fourth state via two channels. By investigating various initial states of the atom and considering the presence or absence of quantum interference in spontaneous emission channels, we analyze how the characteristics of the OAM-carrying vortex beam imprint onto the emission spectrum. The interplay between the optical vortex and the quantum system, including its environment modes, induces a wide variety of spatiospectral behavior, including two-dimensional spectral-peak narrowing, spectral-peak enhancement, spectral-peak suppression, and spontaneous emission reduction or quenching in the spatial azimuthal plane. Our findings shed light on the dynamics of atom–vortex-beam light interactions and offer insights into the manipulation of emission properties at the quantum level.

I. INTRODUCTION

There has been a notable surge in the study of spontaneous emission resulting from the interplay between quantum systems and environmental modes [1,2]. Considering various methods and systems aimed at manipulating and controlling the spectrum of spontaneous emission has evolved into a captivating frontier within the realm of scientific research. Extensive efforts have been invested in delving into theoretical frameworks that address the control of spontaneous emission [3–20]. The applications stemming from the control of spontaneous emission are multifaceted, spanning diverse areas such as lasing without inversion [21,22], electromagnetically induced grating (EIG) [23,24], accurate localization and magnetic field measurement [8,25–27], transparent materials with a high refractive index [28,29], and advanced quantum information processing [30,31]. The manipulation of spontaneous emission has been demonstrated through various approaches, including spontaneously generated coherence [32], relative phase control [6], control through incoherent pump processes

[33], external coupling-field control [7,14], and altering the environmental conditions of atoms, such as in free space [34], in proximity to plasmonic nanostructures [35], within photonic crystals [36], and in confinement within optical cavities [37]. Each case presents unique densities of electromagnetic modes interacting with matter, showcasing the versatility of the control mechanisms associated with spontaneous emission in quantum systems.

At the same time, optical vortices, known for carrying orbital angular momentum (OAM) [38,39], have recently garnered increased attention due to their promising applications across various domains. Optical vortices exhibit distinctive characteristics, featuring helical wave fronts that converge into circular patterns, deviating from conventional point focuses. The spotlight has particularly intensified on these twisted light beams, showcasing their potential in quantum information processing [40], biosciences [41], microtrapping and alignment [42], and optical micromanipulation [43]. However, to comprehensively understand their impact, it is imperative to delve into the unique nature of the interaction between optical vortices and matter. The interplay between these unique structured light beams and matter reveals a multitude of captivating phenomena and effects, which have been extensively investigated [44–61].

Recently, optical vortices endowed with OAM ushered in a novel realm of possibilities for manipulating electromagnetically induced transparency (EIT) [62]. This entails the creation of spatially dependent EIT within a phase-dependent

*Contact author: asadpour@ipm.ir
†Contact author: muqaddarabbas@xjtu.edu.cn
‡Contact author: hamid.hamedi@tfai.vu.lt
§Contact author: julius.ruseckas@gmail.com
‖Contact author: paspalak@upatras.gr
¶Contact author: asgari@ipm.ir

033706-1

Λ scheme [50], where the phase sensitivity is meticulously tuned using an external magnetic field. We proposed a sophisticated extension to this spatially dependent EIT, replacing the conventional magnetic field with additional optical transitions [52]. Subsequent studies revealed that optical vortices exert profound spatial effects in EIG [55] and light amplification without inversion [63].

This paper delves into harnessing the inherent OAM in optical vortices for precise spatiospectral control over spontaneous emission in a four-level atom-light coupling system. The system consists of a ground level coupled to two excited states connected with two laser fields, forming a V subsystem. We specifically consider one of the laser beams to be an optical vortex. The upper states decay to a common fourth state through two decay channels. Various scenarios are explored for the initial state of the atom, encompassing cases where the atom (i) initiates from its ground state, (ii) begins in a superposition of excited states, or (iii) undergoes initial oscillations in a superposition involving all three states of the V model. Quantum interference of spontaneous emission channels is also integrated into our analysis. Our findings reveal that the initial state of the atom significantly influences the potential for achieving two-dimensional (2D) spatially dependent spontaneous emission. In case (i), when the atom is initially in its ground level, without the presence of quantum interference, no azimuthal dependence is observed in the emission spectrum. However, the introduction of interference dramatically modifies the scenario, enabling the imprinting of OAM features from the vortex beam onto the emission spectrum. This is attributed to quantum interference closing the level transitions initiated at the ground level, forming a closed loop. The situation differs for cases (ii) and (iii), in which the spatial features of OAM are transferred to the spontaneous emission spectrum either with or without quantum interference. Nevertheless, the presence of interference enhances the results, enabling a diverse range of spatiospectral behaviors, including 2D spectral-peak narrowing, spectral-peak enhancement, spectral-peak elimination, and spontaneous emission reduction or quenching in the spatial azimuthal plane. This research provides valuable insights into azimuthal control of spontaneous emission through OAM manipulation in optical vortex interactions with multilevel atomic systems.

Spatial control of spontaneous emission spectra is paramount for precision engineering and customizing the interaction dynamics between atoms and photons. In quantum information processing, it enables efficient quantum gates and enhances computational capabilities through the precise shaping of emission spectra. In enhanced light-matter interactions, spatially controlled emission spectra contribute to advanced devices in quantum optics and cavity quantum electrodynamics, offering tailored interactions for applications like advanced spectroscopy and imaging. The importance extends to quantum sensing and metrology, in which spatial control enhances measurement precision and facilitates accurate quantum state detection. Additionally, in optical communication, creating specialized optical sources with unique spectral properties enhances efficiency and security.

It is noteworthy that a closely related scheme was recently proposed to investigate the generation and detection of optical
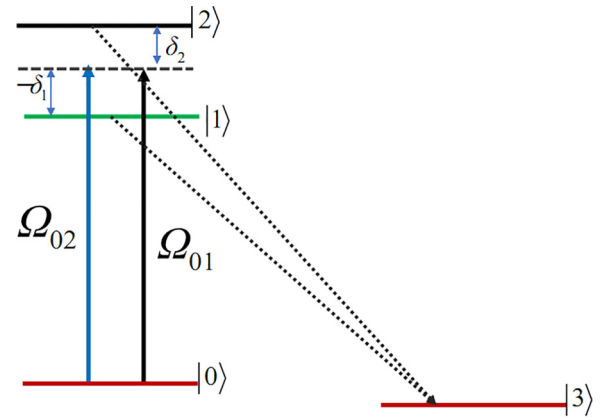

FIG. 1. Illustration of a four-level atomic system in which the ground state is denoted as $|0\rangle$, coupled to two upper states, $|1\rangle$ and $|2\rangle$, via interaction with two laser fields characterized by Rabi frequencies Ω_{01} and Ω_{02}. The upper states exclusively decay to a common state $|3\rangle$.

vortices through spontaneous emission spectra using M-type atoms [64]. In our V-type atomic system, the spontaneous emission of light exhibits heightened efficiency compared to an M-type atomic system, primarily due to the distinctive energy-level configuration of the involved atoms. Within the V-type atomic system, the configuration involves transitions from a singular lower energy level to two distinct higher energy levels. This unique arrangement facilitates a more efficient and precisely controlled emission of light compared to the M-type scheme. The latter entails the superposition of ground-state levels, a task that poses challenges to experimental achievement due to technical limitations and inherent complexities. On the other hand, our proposed scheme is specifically designed to achieve spatiospectral control over spontaneous emission, showcasing a wide range of behaviors. They include two-dimensional spectral-peak narrowing, spectral-peak enhancement, spectral-peak suppression, and spontaneous emission reduction or quenching in the spatial azimuthal plane—effects that were not discussed in Ref. [64].

This paper is organized as follows. In Sec. II, we begin our theoretical exploration by elucidating the system configuration and introducing an azimuthally dependent OAM. In Sec. III, we present the solutions detailing the spatial dependence of the spontaneous emission spectrum across various initial states of the atom. Through rigorous examination, we uncover the intricate interplay between the atomic structure and the characteristics of emitted light. Finally, Sec. IV concludes with a summary of our main conclusions and a discussion of their implications, providing insight into the manipulation of emission properties and possible uses of azimuthal control in quantum systems.

II. THEORY

We consider an atom fixed in position, characterized by a four-level atomic configuration consisting of two lower levels, $|0\rangle$ and $|3\rangle$, and two upper levels, $|1\rangle$ and $|2\rangle$, as illustrated in Fig. 1. In addition one optical vortex light with Rabi frequency $\Psi_{01}(r, \phi)$ and a coupling light with Rabi frequency Ψ_{02}

act on transitions $|0\rangle \rightarrow |1\rangle$ and $|0\rangle \rightarrow |2\rangle$, respectively. The interaction Hamiltonian within the dipole and rotating-wave approximation, considering two structured waves and coupling fields that drive distinct atomic transitions, is expressed as follows:

$$H_I = \hbar\{\Omega_{01}(r,\phi)e^{i\delta_1 t}|0\rangle\langle 1| + \Omega_{02}e^{i\delta_2 t}|0\rangle\langle 2|\}$$
$$+ \sum_k \{g_{\mathbf{k}_1}e^{i(\omega_{13}-\nu_k)t}a_k|1\rangle\langle 3| + g_{\mathbf{k}_2}e^{i(\omega_{23}-\nu_k)t}a_k|2\rangle\langle 3|\}$$
$$+ \text{H.c.},\tag{1}$$

where a_k ($a_k^\dagger$) is the creation (annihilation) operator of the reservoir modes with frequency $\nu_k = ck$ and $g_{\mathbf{k}_1}$ ($g_{\mathbf{k}_2}$) denotes the coupling constant between the vacuum field and the corresponding atomic transition. The last two terms represent spontaneous emission events, during which photons are emitted in random directions with any polarization. The resonant transition frequencies are ω_{13} and ω_{23}. However, the first two terms denote stimulated absorptions of laser photons followed by excitation of the atom. The detunings from states $|1\rangle$ and $|2\rangle$ are denoted by δ_1 and δ_2 ($\delta_{1(2)} = \omega_{1(2)} - \omega_0 - \omega$), where the radiative shifts are omitted. The coupling between the atom and the electromagnetic vacuum field plays a pivotal role in shaping the dynamics of this evolution. Given that the driving field carries optical vortices, the Rabi frequency can be defined as follows:

$$\Omega_{01}(r,\phi) = O_{01}\left(\frac{r}{w}\right)^{|l|}e^{-\frac{r^2}{w^2}}e^{il\phi},\tag{2}$$

where $r = \sqrt{x^2 + y^2}$ represents the radial distance from the beam axis. Here, ϕ signifies the azimuthal angle, and l is an integer corresponding to the OAM of light. Additionally, the parameter w characterizes the beam waist, and O_{01} quantifies the strength of the vortex and coherent fields. Furthermore, $\Omega_{01}(r,\phi) = \Omega_{10}^*(r,\phi)$, indicating that $\Omega_{10}(r,\phi) = O_{10}(\frac{r}{w})^{|l|}e^{-\frac{r^2}{w^2}}e^{-il\phi}$ and $O_{10} = O_{01}$. In contrast, Ω_{02} is treated as a real constant ($\Omega_{02} = \Omega_{20}$), devoid of any spatial dependence. This deliberate choice sets the stage, allowing us to introduce OAM properties of light into the spontaneous emission spectrum. In the next section, we explore the spatial characteristics introduced by the azimuthal dependence induced by Ω_{01}. This intentional choice of the state of the light beams serves as a foundation for imparting OAM properties to the spontaneous emission spectrum. We will explore the spatial characteristics that emerge from the azimuthal dependence induced by Ω_{01} on the spontaneous emission of light.

The state vector of the atom-field system under consideration at time t, whose evolution is governed by the Schrödinger equation, can be expressed as

$$|\Psi(t)\rangle = \int dr f(r)|r\rangle\Big\{[b_0(t)|0\rangle + b_1(t)|1\rangle + b_2(t)|2\rangle]|\{0\}\rangle$$
$$+ \sum_k b_{\mathbf{k}}(t)|3\rangle|1_k\rangle\Big\},\tag{3}$$

where the probability amplitude $b_i(t)$ ($i = 0, 1, 2$) represents the state of the atom at time t when there is no spontaneously emitted photon, $b_{\mathbf{k}}(t)$ is the probability amplitude that the atom is in level $|3\rangle$ with one photon emitted spontaneously in the kth vacuum mode, and $f(r)$ is the center-of-mass wave function of the atom. In the following calculations, $f(r)$ is presumed to be nearly constant across numerous wavelengths of the vortex light, and it remains unchanged even after interacting with the driving field. The probability amplitude $b_{\mathbf{k}}(t \rightarrow \infty)$ can be obtained by solving the Schrödinger wave equation with the interaction Hamiltonian (1) and the atom-field state vector (3). Making use of the Weisskopf-Wigner theory [65], the dynamical equations governing the atomic probability amplitudes, with $\hbar$ set to 1 [6], are given by

$$i\dot{b}_0(t) = \Omega_{10}(r,\phi)b_1(t) + \Omega_{20}(r,\phi)b_2(t),\tag{4}$$

$$i\dot{b}_1(t) = \Omega_{10}(r,\phi)b_0(t) + \left(\delta_1 - i\frac{\Gamma_1}{2}\right)b_1(t) - ip\frac{\sqrt{\Gamma_1\Gamma_2}}{2}b_2(t),\tag{5}$$

$$i\dot{b}_2(t) = \Omega_{20}b_0(t) - ip\frac{\sqrt{\Gamma_1\Gamma_2}}{2}b_1(t) + \left(\delta_2 - i\frac{\Gamma_2}{2}\right)b_2(t),\tag{6}$$

$$i\dot{b}_{\mathbf{k}}(t) = \delta_{\mathbf{k}}b_{\mathbf{k}}(t) - ig_{\mathbf{k}_1}b_1(t) - ig_{\mathbf{k}_2}b_2(t).\tag{7}$$

Additionally, $\delta_{\mathbf{k}} = \omega_{\mathbf{k}} - \omega + \omega_3 - \omega_0$ and $\Gamma_s = 2\pi|g_{\mathbf{k}_s}|^2 D(\omega_{s3})$ for $s = 1, 2, 3, 4$ represent the spontaneous decay rates of states $|1\rangle$ and $|2\rangle$, respectively. Here, $\mathbf{k}$ denotes both the momentum vector and the polarization of the emitted photon. The parameter $D(\omega_{s3})$ signifies the mode density at frequency ω_{s3}. The alignment (of the two dipole moment matrix elements $\vec{\mu}_{ns}$, with $n = 1, 2, s = 3$) parameter p, defined as $p = \vec{\mu}_{13} \cdot \vec{\mu}_{23}/|\vec{\mu}_{13}||\vec{\mu}_{23}|$, plays a pivotal role in spontaneous emission cancellation [6].

Spontaneous emission spectrum

The (long-time) spontaneous emission spectrum $S(\delta_{\mathbf{q}})$ is expressed as $S(\delta_{\mathbf{k}})/S_0 = |b_{\mathbf{k}}(t \rightarrow \infty)|^2$, where $S_0 = D(\omega_{s3})$ [6]. We employ the Laplace transform method to calculate $b_{\mathbf{k}}(t \rightarrow \infty)$ [66]. Utilizing Eqs. (5)–(7) and the final value theorem, we derive the expression

$$b_{\mathbf{k}}(t \rightarrow \infty) = -\frac{g_{\mathbf{k}_1}M(\delta_{\mathbf{q}}) + g_{\mathbf{k}_2}N(\delta_{\mathbf{q}})}{Z(\delta_{\mathbf{k}})},\tag{8}$$

where the coefficients $M(\delta_{\mathbf{q}})$, $N(\delta_{\mathbf{q}})$, and $Z(\delta_{\mathbf{k}})$ are given by

$$M(\delta_{\mathbf{k}}) = ib_0(0)\xi_0 + ib_1(0)\xi_1 - ib_2(0)\xi_2,\tag{9}$$

$$N(\delta_{\mathbf{k}}) = ib_0(0)\xi_3 - ib_1(0)\xi_4 + ib_2(0)\xi_5,\tag{10}$$

$$Z(\delta_{\mathbf{k}}) = \Lambda + ip\frac{\sqrt{\Gamma_1\Gamma_2}}{2}(\Omega_{10}\Omega_{02} + \Omega_{01}\Omega_{20}),\tag{11}$$

with $\xi_0 = \Omega_{10}X_2 - i\Omega_{20}p\frac{\sqrt{\Gamma_1\Gamma_2}}{2}$, $\xi_1 = \delta_{\mathbf{q}}X_2 - |\Omega_{02}|^2$, $\xi_2 = i\delta_{\mathbf{k}}p\frac{\sqrt{\Gamma_1\Gamma_2}}{2} - \Omega_{10}\Omega_{02}$, $\xi_3 = \Omega_{20}X_1 - i\Omega_{10}p\frac{\sqrt{\Gamma_1\Gamma_2}}{2}$, $\xi_4 = i\delta_{\mathbf{k}}p\frac{\sqrt{\Gamma_1\Gamma_2}}{2} - \Omega_{01}\Omega_{20}$, $\xi_5 = \delta_{\mathbf{k}}X_1 - |\Omega_{01}|^2$, $X_1 = \delta_{\mathbf{k}} - \delta_1 + i\frac{\Gamma_1}{2}$, $X_2 = \delta_{\mathbf{k}} - \delta_2 + i\frac{\Gamma_2}{2}$, and $\Lambda = \delta_{\mathbf{k}}(X_1X_2 + p^2\frac{\Gamma_1\Gamma_2}{4}) - (|\Omega_{01}|^2X_2 + |\Omega_{02}|^2X_1)$. In this case, the spontaneous emission

spectrum $S(\delta_{\mathbf{k}})/S_0$ is given by

$$
\begin{aligned}
\frac{S(\delta_{\mathbf{k}})}{S_0} &= |b_{\mathbf{k}}(t \to \infty)|^2 = \left| \frac{g_{\mathbf{k}_1}M(\delta_{\mathbf{k}}) + g_{\mathbf{k}_2}N(\delta_{\mathbf{k}})}{Z(\delta_{\mathbf{k}})} \right|^2 \\
&= g_{\mathbf{k}_1}g_{\mathbf{k}_1}^* \frac{M(\delta_{\mathbf{q}})M^*(\delta_{\mathbf{k}})}{Z(\delta_{\mathbf{k}})Z^*(\delta_{\mathbf{k}})} + g_{\mathbf{k}_2}g_{\mathbf{k}_2}^* \frac{N(\delta_{\mathbf{k}})N^*(\delta_{\mathbf{k}})}{Z(\delta_{\mathbf{k}})Z^*(\delta_{\mathbf{k}})} \\
&\quad + g_{\mathbf{k}_1}g_{\mathbf{k}_2}^* \frac{M(\delta_{\mathbf{k}})N^*(\delta_{\mathbf{k}})}{Z(\delta_{\mathbf{k}})Z^*(\delta_{\mathbf{k}})} + g_{\mathbf{k}_2}g_{\mathbf{k}_1}^* \frac{N(\delta_{\mathbf{k}})M^*(\delta_{\mathbf{k}})}{Z(\delta_{\mathbf{k}})Z^*(\delta_{\mathbf{k}})},
\end{aligned}
\tag{12}
$$

where $g_{\mathbf{k}_1}g_{\mathbf{k}_1}^* \propto \Gamma_1$, $g_{\mathbf{k}_2}g_{\mathbf{k}_2}^* \propto \Gamma_2$, and $g_{\mathbf{k}_1}g_{\mathbf{k}_2}^* = g_{\mathbf{k}_2}g_{\mathbf{k}_1}^* \propto p\sqrt{\Gamma_1\Gamma_2}$ [33]. In all the following simulations, we take $g_{\mathbf{k}_1} = g_{\mathbf{k}_2} = 1$ [7].

III. SPATIALLY DEPENDENT SPONTANEOUS EMISSION

We discuss the phenomenon of spatially dependent spontaneous emission in this section, paying particular attention to the modification of OAM in the composite vortex light across several atom starting states. We also investigate the evolution of the emission properties to the different atomic quantum states in terms of quantum interference. The dynamic interaction between atoms and light will be examined by analyzing the spectral spot patterns in the emission spectrum.

Equation (12), along with Eqs. (9)–(11), highlights the profound sensitivity of spontaneous emission to the initial state of the atom. Subsequent analysis explores various potential initial states for the atom. This includes scenarios in which the atom is initially in its ground state $|0\rangle$, the atom starts in the superposition of excited states $|1\rangle$ and $|2\rangle$, and the atom initially oscillates in the superposition of states $|0\rangle$, $|1\rangle$, and $|2\rangle$. The investigation meticulously assesses the impact of the OAM of light on spontaneous emission in each distinctive scenario. Our analysis comprehensively considers situations both with and without the quantum interference term p.

A. Ground state |0⟩ as the initial state

Upon assuming that the system's initial state is the ground state $|0\rangle$, characterized by $b_0(0) = 1$, $b_1(0) = b_2(0) = 0$, and the quantum interference term p being null ($p = 0$), the results gleaned from Eqs. (8) through (11) reduce to

$$
M(\delta_{\mathbf{k}}) = ib_0(0)\xi_0 = i\Omega_{10}X_2, \quad N(\delta_{\mathbf{k}}) = ib_0(0)\xi_3 = i\Omega_{20}X_1,
$$

$$
Z(\delta_{\mathbf{k}}) = \delta_{\mathbf{k}}X_1X_2 - (|\Omega_{01}|^2X_2 + |\Omega_{02}|^2X_1).
\tag{13}
$$

In this particular scenario, where $p = 0$, the final two components in Eq. (12) vanish. Consequently, only the initial two terms contribute to the spontaneous emission spectrum. Therefore, the expression for the spontaneous emission spectrum simplifies to

$$
\frac{S(\delta_{\mathbf{k}})}{S_0} = \frac{|\Omega_{01}|^2X_2X_2^*}{Z(\delta_{\mathbf{k}})Z^*(\delta_{\mathbf{k}})} + \frac{|\Omega_{02}|^2X_1X_1^*}{Z(\delta_{\mathbf{k}})Z^*(\delta_{\mathbf{k}})}.
\tag{14}
$$

We can find from Eq. (14) that the spontaneous emission spectrum depends significantly on only the intensity distribution of the applied lights. In this case, we have only a spatial distribution of the spontaneous emission spectrum without any dependence on the OAM of the optical beam Ω_{01}. As a result, $S(\delta_{\mathbf{k}})$ remains unaffected by the OAM in the presence

of the vortex beam Ω_{01}. This insensitivity arises because the square magnitude of the field is the only term present in the expression for the spontaneous emission spectrum and it does not incorporate the phase factor $e^{\pm il\phi}$.

In the presence of quantum interference p, however, the scenario undergoes a significant transformation. Notably, the expressions for $M(\delta_{\mathbf{q}})$ and $N(\delta_{\mathbf{k}})$ become

$$
M(\delta_{\mathbf{k}}) = ib_0(0)\xi_0 = i\left(\Omega_{10}X_2 - i\Omega_{20}p\frac{\sqrt{\Gamma_1\Gamma_2}}{2}\right),
$$

$$
N(\delta_{\mathbf{k}}) = ib_0(0)\xi_3 = i\left(\Omega_{20}X_1 - i\Omega_{10}p\frac{\sqrt{\Gamma_1\Gamma_2}}{2}\right),
\tag{15}
$$

and the equation for $Z(\delta_{\mathbf{k}})$ remains consistent with Eq. (11). All four components in Eq. (12) actively contribute to shaping the spontaneous emission spectrum, revealing a discernible dependence on the phase factor $e^{il\phi}$ (or $e^{-il\phi}$).

In this particular scenario, the angular momentum dependence of $S(\delta_{\mathbf{k}})$ now arises from the direct term of Ω_{01}, which appears in $M(\delta_{\mathbf{k}})M^*(\delta_{\mathbf{k}})$, $N(\delta_{\mathbf{k}})N^*(\delta_{\mathbf{k}})$, and $Z(\delta_{\mathbf{k}})Z^*(\delta_{\mathbf{k}})$ in Eq. (12). This indicates that the spontaneously emitted photon acquires OAM characteristics of the vortex beam, signifying a transfer of the OAM from the laser beam Ω_{01} to the spontaneously emitted photon. The imprinting of vortices onto the spontaneously emitted photon can be detected by mapping the spontaneous emission spectrum $S(\delta_{\mathbf{k}})$, as we will illustrate in the following numerical results. The sensitivity of $S(\delta_{\mathbf{k}})$ to the OAM of the beam Ω_{01} arises from the phase-dependent nature of the four-level system. This sensitivity becomes apparent when the system is initially prepared with $b_0(0) = 1$ and $b_1(0) = b_2(0) = 0$ in the presence of quantum interference. Consequently, the spectrum $S(\delta_{\mathbf{k}})$ becomes dependent on the azimuthal angle ϕ of the vortex beam carrying the OAM. This sensitivity can be harnessed to measure regions of spatially varying spontaneous emission by examining $S(\delta_{\mathbf{k}})$. Furthermore, it provides a promising avenue for identifying the winding number of a vortex beam by mapping the spatially dependent spontaneous emission spectrum.

Figure 2 depicts the 2D spontaneous emission spectrum $S(\delta_{\mathbf{k}})$ of an atom initially in the ground state across various vorticities in the x-y plane. Figure 2(a) shows a scenario with degenerate upper states $\omega_{21} = 0$, while Fig. 2(b) presents a nondegenerate case $\omega_{21} = 2\Gamma$, where $\omega_{21} = \delta_2 - \delta_1$ represents the energy splitting of upper states. Throughout all simulations, we maintain $\Gamma_1 = \Gamma_2 = \Gamma$, and all parameters are scaled by Γ. The dark-red structures in Fig. 2 denote positions of spontaneous emission enhancement or 2D spectral peaks, while the blue areas correspond to regions causing quenching or reduction in spontaneous emission in the 2D azimuthal plane. In Fig. 2(a), which depicts the degenerate case, a 2D spectral peak for $l = 1$ is embedded in regions of zero spontaneous emission. The profile of $S(\delta_{\mathbf{k}})$ exhibits an l-fold symmetry. Increasing the winding number to larger values augments the number of 2D spectral spots while simultaneously modifying their amplitude and width. The width of the 2D spectral peaks is consistently reduced with increasing l, indicating that larger l values result in the narrowing of the spectral peaks. Notably, the enhancement of 2D spectral peaks is also observed for $l = 4$ [see Fig. 2(a), panel (iv)].
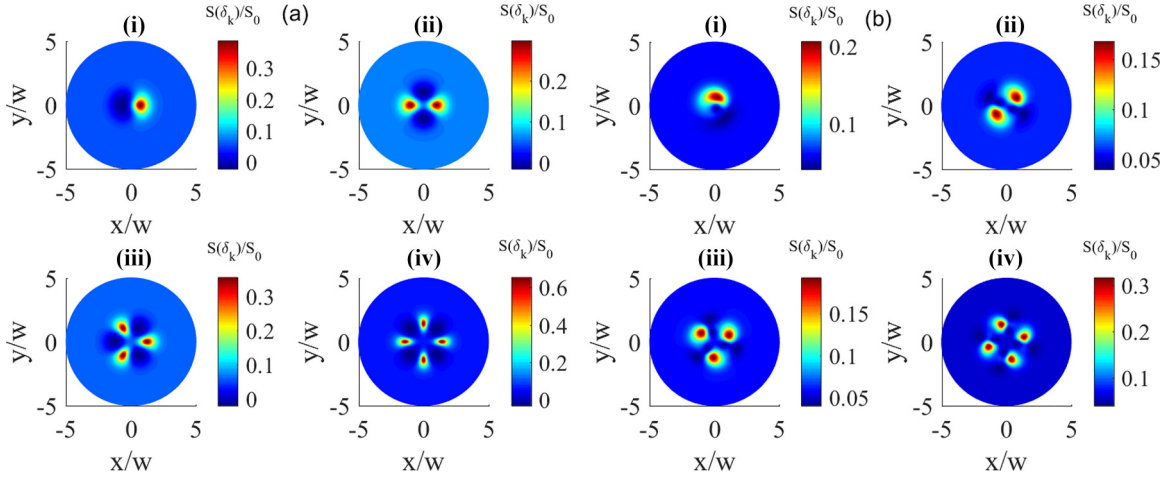
FIG. 2. Azimuthal modulation of the spontaneous emission $S(\delta_{\mathbf{k}})/S_0$ for the first initial condition where $b_0(0) = 1$ and $b_1(0) = b_2(0) = 0$ in the presence of the quantum interference term p ($p = 1$) for (i) $l = 1$, (ii) $l = 2$, (iii) $l = 3$, and (iv) $l = 4$. In (a) $\delta_1 = \delta_2 = 0$, and hence, $\omega_{21} = 0$. In (b) $\delta_1 = -\delta_2 = -\Gamma$, and hence, $\omega_{21} = 2\Gamma$. The other parameters are $\delta_{\mathbf{k}} = 0$, $\Omega_{02} = O_{01} = \Gamma$, and $\Gamma_1 = \Gamma_2 = \Gamma$.

Consequently, determining an unknown vorticity of a beam Ω_{01} becomes straightforward by counting the spectral spot structures in the $S(\delta_{\mathbf{k}})$ spectrum. Moreover, the spatially dependent suppression of spontaneous emission can be established while simultaneously modifying the width and amplitude of the 2D spectral peaks by tuning the topological charge l. Similar trends are observed for the nondegenerate case, as shown in Fig. 2(b). However, the entire spontaneous emission spectrum is observed to rotate counterclockwise in comparison to Fig. 2(a). The spatial control observed in the spontaneous emission spectrum, leading to regions of spectral-peak narrowing or enhancement and quenching of spontaneous emission, directly stems from the transfer of OAM from the vortex beam Ω_{01} to the spontaneous emission.

B. Superposition of excited states |1⟩ and |2⟩ as the initial state

Considering the initial conditions in which the system resides in a superposition of upper states characterized by $b_0(0) = 0$, $b_1(0) = b_2(0) = \frac{1}{\sqrt{2}}$, and a null quantum interference term $p = 0$, we derive expressions for $M(\delta_{\mathbf{k}})$ and $N(\delta_{\mathbf{k}})$ from Eqs. (9)–(11):

$$M(\delta_{\mathbf{k}}) = ib_1(0)\xi_1 - ib_2(0)\xi_2 = \frac{i}{\sqrt{2}}(\xi_1 + \Omega_{10}\Omega_{02}),$$

$$N(\delta_{\mathbf{k}}) = -ib_1(0)\xi_4 + ib_2(0)\xi_5 = \frac{i}{\sqrt{2}}(\xi_5 + \Omega_{01}\Omega_{20}), \quad (16)$$

and $Z(\delta_{\mathbf{k}})$ retains its structure as outlined in Eq. (13). Consequently, we obtain, for $S(\delta_{\mathbf{k}})$,

$$S(\delta_{\mathbf{k}}) \propto |b_{\mathbf{k}}(t \to \infty)|^2 = \frac{\xi_1\xi_1^* + \xi_5\xi_5^* + \Omega_{01}\Omega_{20}(\xi_1 + \xi_1^*) + \Omega_{10}\Omega_{02}(\xi_1^* + \xi_5) + 2|\Omega_{01}|^2|\Omega_{02}|^2}{2Z(\delta_{\mathbf{k}})Z^*(\delta_{\mathbf{k}})}. \quad (17)$$

In this case, even when $p = 0$, as indicated by Eq. (17), a pronounced effect of the optical beam's OAM is evident. This effect is noticeable owing to the presence of the terms $\Omega_{10}\Omega_{02}$ and $\Omega_{10}\Omega_{02}$ in the numerator of Eq. (17). The azimuthally dependent spontaneous emission $S(\delta_{\mathbf{k}})$ for this specific case is showcased in Figs. 3(a) and 3(b) for degenerate and nondegenerate scenarios, respectively, and varying vortex numbers. Figures 3(a) and 3(b) distinctly illustrate the transference of OAM from the vortex beam to the spontaneous emission spectrum in the absence of p. Upon closer examination of Fig. 3(a), it becomes apparent that both 2D spectral-peak enhancements (highlighted by red spots) and 2D spectral-peak suppressions (indicated by blue spots) manifest. These phenomena emerge within a backdrop of moderate spontaneous emission (highlighted in the green zone). The number of these enhancements and suppressions increases with the elevation of the charge l, coupled with a narrowing of their respective widths. The trends observed for the nondegenerate case are similar, except

that in this case spontaneous emission does not completely diminish to zero.

Exploring a different regime of interest for the initial condition in which the atom initially resides in a superposition of upper states, we turn our attention to the presence of quantum interference. While the analytical solutions for $S(\delta_{\mathbf{k}})$ are not provided here due to their extensive nature and lack of inherent informativeness, they can be directly derived from Eqs. (8)–(12) by setting $b_0(0) = 0$, $b_1(0) = b_2(0) = \frac{1}{\sqrt{2}}$, and $p \neq 0$. Opting for maximum quantum interference with $p = 1$ (like in Fig. 2) we examine in Fig. 4 how interference in this case introduces modifications to the spatially dependent spontaneous emission spectra. Figure 4 distinctly reveals the preservation of l-fold symmetry in the spectral spots. Particularly noteworthy is the outcome for the degenerate case $\omega_{21} = 0$ and $l = 4$, where the 2D spectral peak experiences significant enhancement alongside a narrowing of the spectral peak [Fig. 4(a), panel (iv)]. Conversely, in the nondegenerate
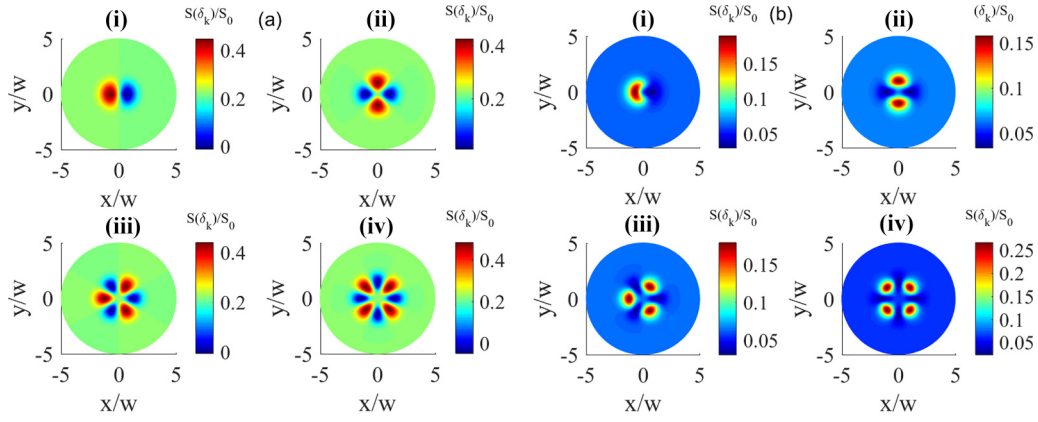
FIG. 3. Azimuthal modulation of the spontaneous emission $S(\delta_{\mathbf{k}})/S_0$ for the second initial condition where $b_0(0) = 0$ and $b_1(0) = b_2(0) = \frac{1}{\sqrt{2}}$ in the absence of the quantum interference term p ($p = 0$) for (i) $l = 1$, (ii) $l = 2$, (iii) $l = 3$, and (iv) $l = 4$. In (a) $\delta_1 = \delta_2 = 0$, and hence, $\omega_{21} = 0$. In (b) $\delta_1 = -\delta_2 = -\Gamma$, and hence, $\omega_{21} = 2\Gamma$. The other parameters are $\delta_{\mathbf{k}} = 0$, $\Omega_{02} = O_{01} = \Gamma$, and $\Gamma_1 = \Gamma_2 = \Gamma$.

case $\omega_{21} = 2\Gamma$ [Fig. 4(b)], the spectral peaks undergo a counterclockwise rotation once again.

C. Superposition of $|0\rangle$, $|1\rangle$, and $|2\rangle$ states as the initial state

For a generic scenario, where the atom is initially distributed among all three states $|0\rangle$, $|1\rangle$, and $|2\rangle$, the solutions for this case were presented in Eqs. (8)–(12). Figures 5 and 6 illustrate the simulation results for the 2D spatially dependent spontaneous emission in this context, considering $p = 0$ and $p = 1$, respectively. Figures 5(a) and 6(a) depict the degenerate case, while Figs. 5(b) and 6(b) showcase the nondegenerate case.

For this initial superposition state preparation of the atom, the spontaneous emission again exhibits spatial dependence in both the absence and presence of quantum interference p, imprinting the OAM characteristics of the vortex beam onto the spectrum of $S(\delta_{\mathbf{k}})$. Particularly interesting phenomena, such as 2D spectral-peak narrowing and spectral-peak enhancement [see, e.g., Fig. 6(a), panel iv], spectral-peak suppression [see, e.g., Fig. 5(a)], and spontaneous emission reduction or quenching in the azimuthal plane, can be observed. All these effects are achievable by varying the vorticity number l.

Interestingly, for $p = 0$ ($p = 1$), a clockwise (counterclockwise) rotation of 2D patterns is observed for the nondegenerate case, as shown in Fig. 5(b) [Fig. 6(b)] with respect to the degenerate case illustrated in Fig. 5(a) [Fig. 6(a)].

D. The case with Gaussian beams

Finally, we consider the case where both coupling fields are Gaussian beams with the OAM equal to zero. For this scenario, we analyze the situations depicted in Fig. 7: (i) $p = 0$, $b_0(0) = 1$, and $b_1(0) = b_2(0) = 0$; (ii) $p = 1$, $b_0(0) = 1$, and $b_1(0) = b_2(0) = 0$; (iii) $p = 0$, $b_0(0) = 0$, and $b_1(0) = b_2(0) = \frac{1}{\sqrt{2}}$; and (iv) $p = 1$, $b_0(0) = 0$, and $b_1(0) = b_2(0) = \frac{1}{\sqrt{2}}$. In Fig. 7(a), $\delta_1 = \delta_2 = 0$, resulting in $\omega_{21} = 0$. In Fig. 7(b), $\delta_1 = -\delta_2 = -\Gamma$, leading to $\omega_{21} = 2\Gamma$. The other parameters are $\delta_{\mathbf{k}} = 0$, $\Omega_{02} = \Omega_{01} = \Gamma$, and $\Gamma_1 = \Gamma_2 = \Gamma$.

As illustrated, when Gaussian beams are applied, the spontaneous emission spectrum exhibits no spatial dependence and remains homogeneous in the azimuthal plane. This contrasts with the previous cases involving optical vortices. In scenarios (i) and (ii), where the population initially resides in the ground level [$b_0(0) = 1$, $b_1(0) = b_2(0) = 0$], the patterns display a ring structure with maximum 2D spectral patterns
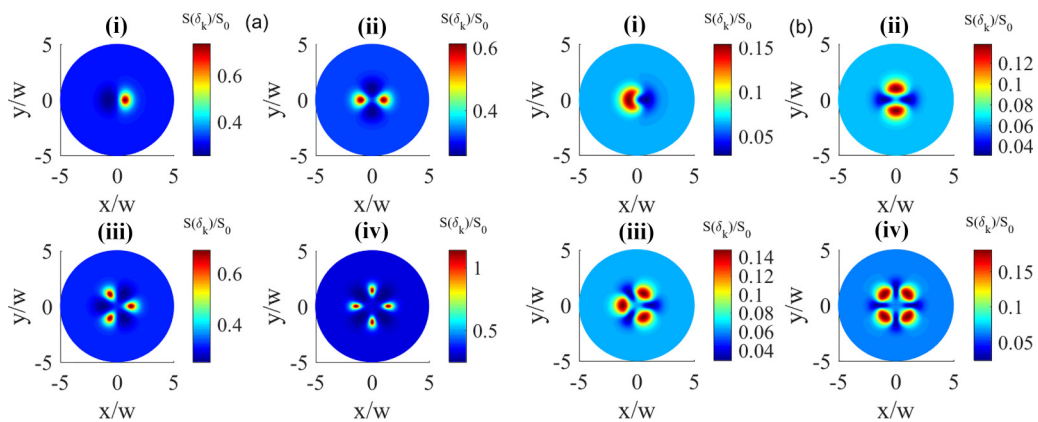

FIG. 4. Azimuthal modulation of the spontaneous emission $S(\delta_{\mathbf{k}})/S_0$ for the last initial condition where $b_0(0) = 0$ and $b_1(0) = b_2(0) = \frac{1}{\sqrt{2}}$ in the presence of the quantum interference term p ($p = 1$) for (i) $l = 1$, (ii) $l = 2$, (iii) $l = 3$, and (iv) $l = 4$. In (a) $\delta_1 = \delta_2 = 0$, and hence, $\omega_{21} = 0$. In (b) $\delta_1 = -\delta_2 = -\Gamma$, and hence, $\omega_{21} = 2\Gamma$. The other parameters are $\delta_{\mathbf{k}} = 0$, $\Omega_{02} = O_{01} = \Gamma$, and $\Gamma_1 = \Gamma_2 = \Gamma$.
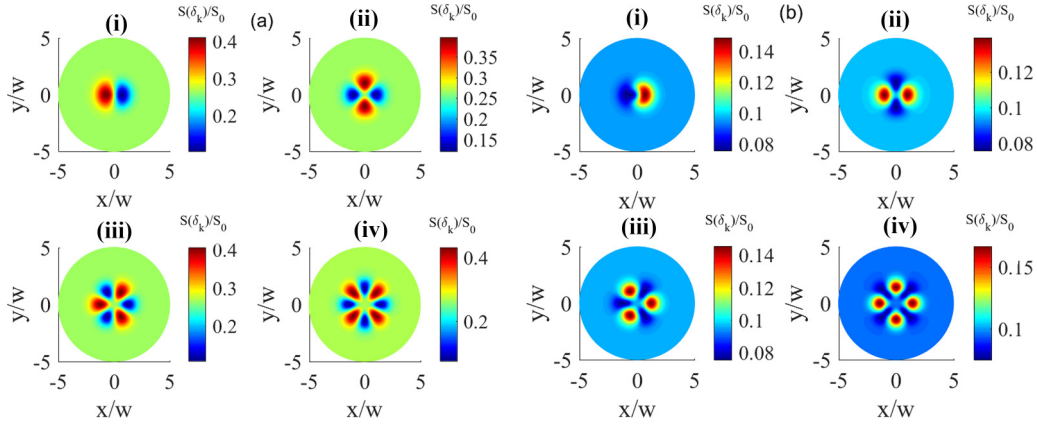
FIG. 5. Azimuthal modulation of the spontaneous emission $S(\delta_{\mathbf{k}})$ for the case where $b_0(0) = b_1(0) = b_2(0) = \frac{1}{\sqrt{3}}$ in the absence of the quantum interference term p ($p = 0$) for (i) $l = 1$, (ii) $l = 2$, (iii) $l = 3$, and (iv) $l = 4$. In (a) $\delta_1 = \delta_2 = 0$, and hence, $\omega_{21} = 0$. In (b) $\delta_1 = -\delta_2 = -\Gamma$, and hence, $\omega_{21} = 2\Gamma$. The other parameters are $\delta_{\mathbf{k}} = 0$, $\Omega_{02} = O_{01} = \Gamma$, and $\Gamma_1 = \Gamma_2 = \Gamma$.

of spontaneous emission occurring in the rings. Conversely, in scenarios (iii) and (iv), where the initial condition is $b_0(0) = 0$ and $b_1(0) = b_2(0) = \frac{1}{\sqrt{2}}$, the patterns show a homogeneous distribution of spontaneous emission in the 2D azimuthal space, with spectral-peak suppression at the core of the azimuthal plane.

Furthermore, the results indicate that nonzero detuning does not affect the overall pattern and changes only the amplitude of the plots, as seen by comparing Figs. 7(a) and 7(b). These findings suggest that the optimal approach to observing spatially dependent spontaneous emission spectra involves using inhomogeneous optical vortex beams, which can transfer their inhomogeneity to the spatiospectral patterns.

E. Further discussions and limitations of the model

In this section, we explore the nature of the observed patterns and the mechanisms behind them. We specifically focus on the cases of spatially dependent spontaneous emission illustrated in Figs. 2–6, in contrast to the spatially independent outcomes observed with Gaussian beams (Fig. 7).

The modifications and rotations observed in Figs. 2–6 primarily arise from the introduction of nonzero detunings in

Figs. 2(b)–6(b) for the nondegenerate cases. These alterations can be interpreted through the analytical solutions of the spontaneous emission spectrum, as described in Eq. (12) for each specific scenario.

Let us assume, for instance, the case in Fig. 2(a), where $\delta_1 = 0$, $\delta_2 = 0$, and $p = 1$, with initial conditions $b_0(0) = 1$ and $b_1(0) = b_2(0) = 0$. In this case, Eq. (12) simplifies to

$$\frac{S(\delta_k = 0)}{S_0} = \frac{1}{2} \frac{|\Omega_{01}|^2 + |\Omega_{02}|^2 - 2\Omega\Omega_{02}\cos(l\phi)}{|\Omega_{01}|^2 + |\Omega_{02}|^2 + 2\Omega\Omega_{02}\cos(l\phi)|^2}, \quad (18)$$

where we have assumed $\Omega_{01} = \Omega e^{il\phi}$, $\Omega_{10} = \Omega e^{-il\phi}$, $\Omega = \Omega_{01}(\frac{r}{w})^{|l|}e^{-\frac{r^2}{w^2}}$, and Ω_{02} is a real constant ($\Omega_{02} = \Omega_{20}$). The term $\cos(l\phi)$ introduces l-fold symmetry, resulting in a sinusoidal modulation of spontaneous emission patterns in Fig. 2(a), indicating that increasing the OAM number l enhances the number of spectral spots.

Analytical solutions of Eq. (12) for the spontaneous emission spectrum for the nondegenerate case with nonzero detuning provide further insights into further modifications of patterns. While detailed expressions are extensive in such cases, a general examination of parameters X_1 and X_2,
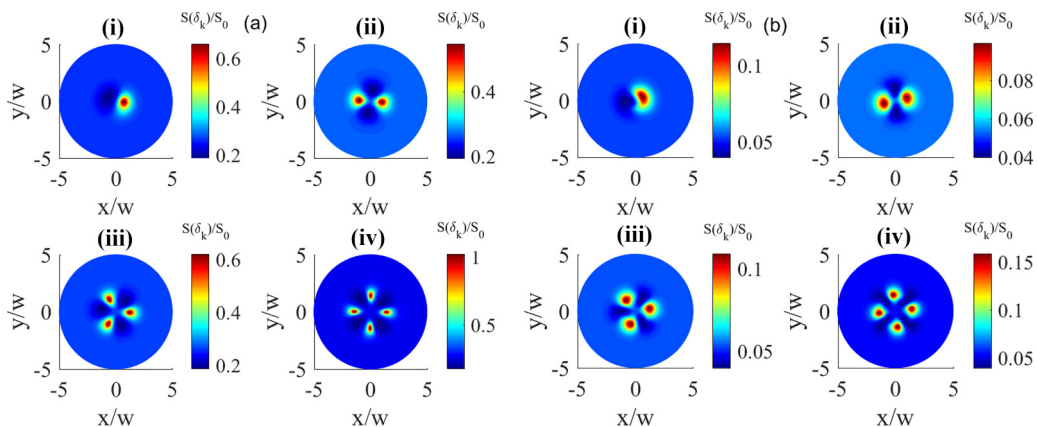

FIG. 6. Azimuthal modulation of the spontaneous emission $S(\delta_{\mathbf{k}})/S_0$ for the case where $b_0(0) = b_1(0) = b_2(0) = \frac{1}{\sqrt{3}}$ in the presence of the quantum interference term p ($p = 1$) for (i) $l = 1$, (ii) $l = 2$, (iii) $l = 3$, and (iv) $l = 4$. In (a) $\delta_1 = \delta_2 = 0$, and hence, $\omega_{21} = 0$. In (b) $\delta_1 = -\delta_2 = -\Gamma$, and hence, $\omega_{21} = 2\Gamma$. The other parameters are $\delta_{\mathbf{k}} = 0$, $\Omega_{02} = O_{01} = \Gamma$, and $\Gamma_1 = \Gamma_2 = \Gamma$.
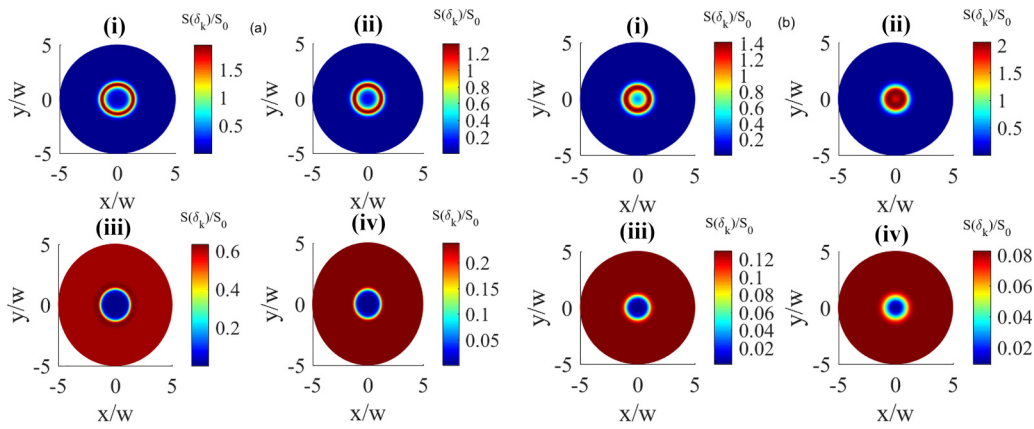
FIG. 7. Azimuthal modulation of the spontaneous emission $S(\delta_{\mathbf{k}})/S_0$ for the case where both beams are Gaussian beams and (i) $p = 0$, $b_0(0) = 1$, and $b_1(0) = b_2(0) = 0$, (ii) $p = 1$, $b_0(0) = 1$, and $b_1(0) = b_2(0) = 0$, (iii) $p = 0$, $b_0(0) = 0$, and $b_1(0) = b_2(0) = \frac{1}{\sqrt{2}}$, and (iv) $p = 1$, $b_0(0) = 0$, and $b_1(0) = b_2(0) = \frac{1}{\sqrt{2}}$. In (a) $\delta_1 = \delta_2 = 0$, and hence, $\omega_{21} = 0$. In (b) $\delta_1 = -\delta_2 = -\Gamma$, and hence, $\omega_{21} = 2\Gamma$. The other parameters are $\delta_{\mathbf{k}} = 0$, $\Omega_{02} = O_{01} = \Gamma$, and $\Gamma_1 = \Gamma_2 = \Gamma$.

defined after Eq. (11), elucidates the rotational nature of these changes. Nonzero detunings for the nondegenerate case introduce real values into these parameters, leading to additional terms in the final spontaneous emission spectrum compared to the degenerate scenario [Eq. (18)]. These additional terms, such as $\Omega_{10}X_2$ via ξ_0, introduce phase factors (e.g., $e^{-il\phi}$), thereby accounting for the observed rotational characteristics of the spectrum. Conversely, terms involving the multiplication of the nonvortex beam Ω_{20} by detuning (e.g., via term ξ_3) modify spectral-peak amplitudes, resulting in either enhancement or reduction of spontaneous emission across the 2D azimuthal plane.

Notably, certain patterns exhibit striking similarities under varied initial conditions. Specifically, in the presence of quantum interference ($p = 1$) and under resonant conditions of the coupling lights ($\delta_i = 0$ for $i = 1, 2$), the spatial patterns of the spontaneous emission spectrum display significant similarity across different values of the OAM and initial conditions [see Figs. 2(a), 4(a) and 6(a)]. The primary distinction lies in the amplitude of the spontaneous emission spectrum in each case, reflecting diverse population distributions in the initial conditions.

Furthermore, scenarios devoid of quantum interference ($p = 0$), where initial states involve superpositions of upper excited states [Figs. 3(a) and 5(a)], reveal similar spatiospectral patterns under resonant conditions of the coupling lights. This similarity arises due to the influence of the initial population in the upper excited states on spatiospectral patterns, common to both scenarios [Figs. 3(a) and 5(a)]. It is important to note that when the initial state is the ground state and $p = 0$, the spontaneous emission spectrum lacks OAM dependence, resulting in the absence of spatiospectral patterns.

Conversely, under off-resonant conditions of the coupling lights ($\delta_1 = -\Gamma$, $\delta_2 = \Gamma$), spatiospectral behaviors of the spontaneous emission spectrum notably differ between scenarios with ($p = 1$) and without ($p = 0$) quantum interference. As discussed earlier, nonzero detuning introduces additional terms in the final spontaneous emission spectrum, such as the modulation of vortex beams Ω_{10} (Ω_{01}) or Ω_{20} by detuning, thereby rotating or modulating the amplitude of the

2D spectra. This variability stems from how initial conditions of the quantum system distribute populations among different states.

In our proposed scheme we have not considered relaxation from excited states $|1\rangle$ and $|2\rangle$ to the ground state $|0\rangle$, which significantly impacts our proposed scheme in multiple ways. Incorporating decay channels from the excited states to the ground state alters population dynamics by enhancing the $|0\rangle$ population, thereby depleting the population available for coherent processes in the excited states, potentially reducing scheme efficiency. Moreover, spontaneous emission from these states to $|0\rangle$ introduces decoherence, diminishing coherence among $|0\rangle$, $|1\rangle$, and $|2\rangle$, which may broaden spectral lines and diminish interference effects in the emission spectrum. Additional spectral lines corresponding to $|1\rangle \rightarrow |0\rangle$ and $|2\rangle \rightarrow |0\rangle$ further complicate spectrum interpretation related to decay to the common state $|3\rangle$. Thus, we initially overlooked relaxation to $|0\rangle$ to focus on spontaneous emission to $|3\rangle$. Mitigating the effects of these relaxation processes may necessitate techniques like optical pumping for population control or methods to suppress decoherence, such as dynamical decoupling.

In our calculation of the spontaneous emission spectrum, we did not consider inhomogeneous broadening, including Doppler broadening. Doppler broadening results from the thermal motion of atoms, causing a spread in resonance frequencies and broadening the spectral lines. This effect reduces the clarity and distinctiveness of spectral features, complicating the identification of individual spatiospectral peaks. Consequently, the interference effects that are crucial to our scheme may become less prominent in the spontaneous emission spectrum. Moreover, Doppler broadening affects the population dynamics of the system. The broadened linewidths imply that not all atoms in the ensemble resonate with the laser fields, leading to varying coupling strengths. This discrepancy can create an uneven distribution of populations across states, disrupting the balance necessary for the optimal operation of the scheme. Since these effects diminish the visibility of our results, we have excluded them from our calculations. To enhance precision and control in

experimental setups, techniques such as magneto-optical trapping (MOT) can be employed to mitigate Doppler broadening by reducing the thermal motion of atoms, as noted in [67]. This approach significantly improves the practical feasibility of our scheme. Additionally, other experimental methods, such as using narrow-linewidth lasers and velocity-selective pumping techniques, can also mitigate the effects of inhomogeneous broadening.

F. Experimental realization of the proposed model

To ensure precise phase control, we recommend employing an optical phase-locked loop approach [68]. Additionally, the effectiveness of our approach is influenced by parameters related to quantum interference terms. Regarding experimental implementation of the proposed setup, we note that quantum interference effects in spontaneous emission have been experimentally observed using bare states of specific atoms [69,70], molecules [71], and semiconductor quantum dots [72].

For the proposal in the present article, one may achieve this experimentally by building on the successful work of Xia *et al.* [71] with sodium dimers. For our purposes, an additional laser would be introduced to facilitate coupling via a four-photon transition. Another suitable platform for this experimental realization is dressed ^{85}Rb (see, for example, Refs. [73,74]). Within this proposal, we can utilize the states $|5P_{1/2}, F = 3\rangle$ and $|5D_{3/2}, F = 4\rangle$ when they are dressed by a laser field as states $|1\rangle$ and $|2\rangle$. Additionally, $|5S_{1/2}, F = 3\rangle$ and $|5S_{1/2}, F = 2\rangle$ of ^{85}Rb can be used as $|0\rangle$ and $|3\rangle$, respectively. Here, $|0\rangle$ represents the ground state, and $|3\rangle$ corresponds to the intermediate state where the spontaneously emitted structured light spectrum is examined. Then, the dressed atomic system interacts with two additional laser fields to create the phenomena in this work. Moreover, another approach is to use a double-dressed InGaAs quantum dot, similar to the work of Ref. [75], to create the necessary quantum interference.

Furthermore, another approach for creating the necessary quantum interference in spontaneous emission is to use the idea of simulating quantum interference effects in spontaneous emission using the anisotropic Purcell effect occurring when a quantum system with orthogonal electric dipole matrix elements is placed in an anisotropic photonic vacuum [76–81].

IV. CONCLUSION

To summarize, our proposed method for achieving spatiospectral control over spontaneous emission in a four-level atom-light coupling system interacting with optical vortices bearing orbital angular momentum revealed a panorama of results. Delving into diverse scenarios and considering the initial state of the atom, this paper has illuminated an array of spatial and spectral behaviors. They encompass intriguing features such as two-dimensional spectral-peak narrowing, enhancement, suppression, and spontaneous emission reduction or quenching spanning the spatial azimuthal plane. The inhomogeneous atom-light interaction, influenced by the optical vortex, intricately structures these effects. The transfer of OAM characteristics onto the emission spectrum not only underscores the potential for azimuthal control of spontaneous emission but also opens avenues for innovative applications in high-dimensional quantum information processing, enhanced communication protocols, and novel sensing technologies. This study enriches comprehension of the dynamics of spatiospectral phenomena and charts a course for applications leveraging precise OAM-based manipulation of spontaneous emission in multilevel atomic systems.

[1] C. C. Gerry and P. L. Knight, *Introductory Quantum Optics* (Cambridge University Press, Cambridge, 2023).

[2] P. Meystre, *Quantum Optics* (Springer, Switzerland, 2021).

[3] P. Zhou and S. Swain, Ultranarrow spectral lines via quantum interference, Phys. Rev. Lett. **77**, 3995 (1996).

[4] S. John and T. Quang, Collective switching and inversion without fluctuation of two-level atoms in confined photonic systems, Phys. Rev. Lett. **78**, 1888 (1997).

[5] P. Zhou and S. Swain, Absorption spectrum and gain without inversion of a driven two-level atom with arbitrary probe intensity in a squeezed vacuum, Phys. Rev. A **55**, 772 (1997).

[6] E. Paspalakis and P. L. Knight, Phase control of spontaneous emission, Phys. Rev. Lett. **81**, 293 (1998).

[7] F. Ghafoor, S.-Y. Zhu, and M. S. Zubairy, Amplitude and phase control of spontaneous emission, Phys. Rev. A **62**, 013811 (2000).

[8] F. Ghafoor, S. Qamar, and M. S. Zubairy, Atom localization via phase and amplitude control of the driving field, Phys. Rev. A **65**, 043819 (2002).

[9] M. A. Antón, O. G. Calderón, and F. Carreño, Spontaneously generated coherence effects in a laser-driven four-level atomic system, Phys. Rev. A **72**, 023809 (2005).

[10] A.-J. Li, J.-Y. Gao, J.-H. Wu, and L. Wang, Simulating spontaneously generated coherence in a four-level atomic system, J. Phys. B **38**, 3815 (2005).

[11] J.-H. Wu, A.-J. Li, Y. Ding, Y.-C. Zhao, and J.-Y. Gao, Control of spontaneous emission from a coherently driven four-level atom, Phys. Rev. A **72**, 023802 (2005).

[12] A. Fountoulakis, A. F. Terzis, and E. Paspalakis, Coherent phenomena due to double-dark states in a system with decay interference, Phys. Rev. A **73**, 033811 (2006).

[13] E. Paspalakis and P. L. Knight, Coherent control of spontaneous emission in a four-level system, J. Mod. Opt. **47**, 1025 (2000).

[14] L. Jia-Hua, L. Ji-Bing, C. Ai-Xi, and Q. Chun-Chao, Spontaneous emission spectra and simulating multiple spontaneous generation coherence in a five-level atomic medium, Phys. Rev. A **74**, 033816 (2006).

[15] R. Arun, Interference-induced splitting of resonances in spontaneous emission, Phys. Rev. A **77**, 033820 (2008).

[16] A.-J. Li, X.-L. Song, X.-G. Wei, L. Wang, and J.-Y. Gao, Effects of spontaneously generated coherence in a microwave-driven four-level atomic system, Phys. Rev. A **77**, 053806 (2008).

[17] C. L. Wang, Z. H. K. S. C. Tian, and J. H. Wu, Control of spontaneous emission from a micro-wave driven atomic system, Opt. Express **20**, 3509 (2012).

[18] I. Thanopulos, V. Karanikolas, and E. Paspalakis, Spontaneous emission of a quantum emitter near a graphene nanodisk under strong light-matter coupling, Phys. Rev. A **106**, 013718 (2022).

[19] I. Thanopulos, V. Karanikolas, N. Iliopoulos, and E. Paspalakis, Non-Markovian spontaneous emission dynamics of a quantum emitter near a MoS$_2$ nanodisk, Phys. Rev. B **99**, 195412 (2019).

[20] C. Whisler, G. Holdman, D. D. Yavuz, and V. W. Brar, Enhancing two-photon spontaneous emission in rare earths using graphene and graphene nanoribbons, Phys. Rev. B **107**, 195420 (2023).

[21] G. S. Agarwal, Inhibition of spontaneous emission noise in lasers without inversion, Phys. Rev. Lett. **67**, 980 (1991).

[22] V. V. Kozlov, Y. Rostovtsev, and M. O. Scully, Inducing quantum coherence via decays and incoherent pumping with application to population trapping, lasing without inversion, and quenching of spontaneous emission, Phys. Rev. A **74**, 063829 (2006).

[23] B. Xie, X. Cai, and Z.-H. Xiao, Electromagnetically induced phase grating controlled by spontaneous emission, Opt. Commun. **285**, 133 (2012).

[24] F. Bozorgzadeh, M. Sahrai, and H. Khoshsima, Controlling the electromagnetically induced grating via spontaneously generated coherence, Eur. Phys. J. D **70**, 191 (2016).

[25] M. O. Scully and M. Fleischhauer, High-sensitivity magnetometer based on index-enhanced media, Phys. Rev. Lett. **69**, 1360 (1992).

[26] R.-G. Wan and T.-Y. Zhang, Two-dimensional sub-half-wavelength atom localization via controlled spontaneous emission, Opt. Express **19**, 25823 (2011).

[27] Z. Wang, J. Chen, and B. Yu, High-dimensional atom localization via spontaneously generated coherence in a microwave-driven atomic system, Opt. Express **25**, 3358 (2017).

[28] M. O. Scully, Enhancement of the index of refraction via quantum coherence, Phys. Rev. Lett. **67**, 1855 (1991).

[29] S. Evangelou, V. Yannopapas, and E. Paspalakis, Transparency and slow light in a four-level quantum system near a plasmonic nanostructure, Phys. Rev. A **86**, 053811 (2012).

[30] C. H. Bennett and D. P. DiVincenzo, Quantum information and computation, Nature (London) **404**, 247 (2000).

[31] M. Paternostro, M. S. Kim, and P. L. Knight, Vibrational coherent quantum computation, Phys. Rev. A **71**, 022311 (2005).

[32] S.-Y. Zhu and M. O. Scully, Spectral line elimination and spontaneous emission cancellation via quantum interference, Phys. Rev. Lett. **76**, 388 (1996).

[33] K. T. Kapale, M. O. Scully, S.-Y. Zhu, and M. S. Zubairy, Quenching of spontaneous emission through interference of incoherent pump processes, Phys. Rev. A **67**, 023804 (2003).

[34] M. Bojer, L. Götzendörfer, R. Bachelard, and J. von Zanthier, Engineering of spontaneous emission in free space via conditional measurements, Phys. Rev. Res. **4**, 043022 (2022).

[35] S. Evangelou, V. Yannopapas, and E. Paspalakis, Modifying free-space spontaneous emission near a plasmonic nanostructure, Phys. Rev. A **83**, 023819 (2011).

[36] H. Z. Zhang, S. H. Tang, P. Dong, and J. He, Quantum interference in spontaneous emission of an atom embedded in a double-band photonic crystal, Phys. Rev. A **65**, 063802 (2002).

[37] G. S. Agarwal and P. K. Pathak, dc-field-induced enhancement and inhibition of spontaneous emission in a cavity, Phys. Rev. A **70**, 025802 (2004).

[38] L. Allen, M. W. Beijersbergen, R. J. C. Spreeuw, and J. P. Woerdman, Orbital angular momentum of light and the transformation of Laguerre-Gaussian laser modes, Phys. Rev. A **45**, 8185 (1992).

[39] S. Franke-Arnold, 30 years of orbital angular momentum of light, Nat. Rev. Phys. **4**, 361 (2022).

[40] J. Wang, F. Castellucci, and S. Franke-Arnold, Vectorial light–matter interaction: Exploring spatially structured complex light fields, AVS Quantum Sci. **2**, 031702 (2020).

[41] D. J. Stevenson, F. G. Moore, and K. Dholakia, Light forces the pace: Optical manipulation for biophotonics, J. Biomed. Opt. **15**, 041503 (2010).

[42] M. P. Macdonald, L. Paterson, K. V. Sepulveda, J. Arlt, W. Sibbett, and K. Dholakia, Creation and manipulation of three-dimensional optically trapped structures, Science **296**, 1101 (2002).

[43] M. Woerdemann, C. Alpmann, M. Esseling, and C. Denz, Advanced optical trapping by complex beam shaping, Laser Photonics Rev. **7**, 839 (2013).

[44] Z. Dutton and J. Ruostekoski, Transfer and storage of vortex states in light and matter waves, Phys. Rev. Lett. **93**, 193602 (2004).

[45] Q.-F. Chen, B.-S. Shi, Y.-S. Zhang, and G.-C. Guo, Entanglement of the orbital angular momentum states of the photon pairs generated in a hot atomic ensemble, Phys. Rev. A **78**, 053810 (2008).

[46] J. Ruseckas, G. Juzeliūnas, P. Öhberg, and S. M. Barnett, Polarization rotation of slow light with orbital angular momentum in ultracold atomic gases, Phys. Rev. A **76**, 053822 (2007).

[47] V. E. Lembessis and M. Babiker, Light-induced torque for the generation of persistent current flow in atomic gas Bose-Einstein condensates, Phys. Rev. A **82**, 051402(R) (2010).

[48] D.-S. Ding, Z.-Y. Zhou, B.-S. Shi, X.-B. Zou, and G.-C. Guo, Linear up-conversion of orbital angular momentum, Opt. Lett. **37**, 3270 (2012).

[49] J. Ruseckas, V. Kudriašov, I. A. Yu, and G. Juzeliūnas, Transfer of orbital angular momentum of light using two-component slow light, Phys. Rev. A **87**, 053840 (2013).

[50] N. Radwell, T. W. Clark, B. Piccirillo, S. M. Barnett, and S. Franke-Arnold, Spatially dependent electromagnetically induced transparency, Phys. Rev. Lett. **114**, 123603 (2015).

[51] S. Sharma and T. N. Dey, Phase-induced transparency-mediated structured-beam generation in a closed-loop tripod configuration, Phys. Rev. A **96**, 033811 (2017).

[52] H. R. Hamedi, V. Kudriasov, J. Ruseckas, and G. Juzeliunas, Azimuthal modulation of electromagnetically induced transparency using structured light, Opt. Express **26**, 28249 (2018).

[53] H. R. Hamedi, J. Ruseckas, E. Paspalakis, and G. Juzeliūnas, Off-axis optical vortices using double-Raman singlet and doublet light-matter schemes, Phys. Rev. A **101**, 063828 (2020).

[54] J. Qiu, Z. Wang, D. Ding, W. Li, and B. Yu, Highly efficient vortex four-wave mixing in asymmetric semiconductor quantum wells, Opt. Express **28**, 2975 (2020).

[55] S. H. Asadpour, T. Kirova, J. Qian, H. R. Hamedi, G. Juzeliunas, and E. Paspalakis, Azimuthal modulation of electromagnetically induced grating using structured light, Sci. Rep. **11**, 20721 (2021).

[56] F. Song, Z. Wang, E. Li, B. Yu, and Z. Huang, Nonreciprocity with structured light using optical pumping in hot atoms, Phys. Rev. Appl. **18**, 024027 (2022).

[57] N. Daloi, P. Kumar, and T. N. Dey, Guiding and polarization shaping of vector beams in anisotropic media, Phys. Rev. A **105**, 063714 (2022).

[58] G. Z. Hamid, R. Hamedi, V. Ahufinger, T. Halfmann, J. Mompart, and G. Juzeliunas, Spatially strongly confined atomic excitation via a two dimensional stimulated Raman adiabatic passage, Opt. Express **30**, 13915 (2022).

[59] H. R. Hamedi, I. A. Yu, and E. Paspalakis, Matched optical vortices of slow light using a tripod coherently prepared scheme, Phys. Rev. A **108**, 053719 (2023).

[60] Y. Chen, Y. Zhou, M. Li, K. Liu, M. F. Ciappina, and P. Lu, Atomic photoionization by spatiotemporal optical vortex pulses, Phys. Rev. A **107**, 033112 (2023).

[61] C. Meng, T. Shui, and W.-X. Yang, Coherent transfer of optical vortices via backward four-wave mixing in a double-Λ atomic system, Phys. Rev. A **107**, 053712 (2023).

[62] M. Fleischhauer, A. Imamoglu, and J. P. Marangos, Electromagnetically induced transparency: Optics in coherent media, Rev. Mod. Phys. **77**, 633 (2005).

[63] H. R. Hamedi, V. Yannopapas, E. Paspalakis, and J. Ruseckas, Spatially patterned light amplification without inversion, Results Phys. **54**, 107135 (2023).

[64] M. Abbas, U. Saleem, Rahmatullah, Y.-C. Zhang, and P. Zhang, Spontaneously generated structured light in a coherently driven five-level M-type atomic system, Phys. Rev. A **109**, 023716 (2024).

[65] G. S. Agarwal, Quantum statistical theories of spontaneous emission and their relation to other approaches, in *Quantum Optics*, edited by G. Höhler, Springer Tracts in Modern Physics, Vol. 70 (Springer, Berlin, Heidelberg, 1974).

[66] S. M. Barnett and P. M. Radmore, *Methods in Theoretical Quantum Optics* (Oxford University Press, Oxford, 1997).

[67] G. Uhlenberg, J. Dirscherl, and H. Walther, Magneto-optical trapping of silver atoms, Phys. Rev. A **62**, 063404 (2000).

[68] F. Friederich, G. Schuricht, A. Deninger, F. Lison, G. Spickermann, and P. Haring, Phase-locking of the beat signal of two distributed-feedback diode lasers to oscillators working in the MHz to THz range, Opt. Express **18**, 8621 (2010).

[69] D. G. Norris, L. A. Orozco, P. Barberis-Blostein, and H. J. Carmichael, Observation of ground-state quantum beats in atomic spontaneous emission, Phys. Rev. Lett. **105**, 123602 (2010).

[70] K. P. Heeg, H.-C. Wille, K. Schlage, T. Guryeva, D. Schumacher, I. Uschmann, K. S. Schulze, B. Marx, T. Kämpfer, G. G. Paulus, R. Röhlsberger, and J. Evers, Vacuum-assisted generation and control of atomic coherences at x-ray energies, Phys. Rev. Lett. **111**, 073601 (2013).

[71] H.-R. Xia, C.-Y. Ye, and S.-Y. Zhu, Experimental observation of spontaneous emission cancellation, Phys. Rev. Lett. **77**, 1032 (1996).

[72] M. V. G. Dutt, J. Cheng, B. Li, X. Xu, X. Li, P. R. Berman, D. G. Steel, A. S. Bracker, D. Gammon, S. E. Economou, R.-B. Liu, and L. J. Sham, Stimulated and spontaneous optical generation of electron spin coherence in charged GaAs quantum dots, Phys. Rev. Lett. **94**, 227403 (2005).

[73] C.-L. Wang, A.-J. Li, X.-Y. Zhou, Z.-H. Kang, J. Yun, and J.-Y. Gao, Investigation of spontaneously generated coherence in dressed states of ^{85}Rb atoms, Opt. Lett. **33**, 687 (2008).

[74] C.-L. Wang, Z.-H. Kang, S.-C. Tian, Y. Jiang, and J.-Y. Gao, Effect of spontaneously generated coherence on absorption in a V-type system: Investigation in dressed states, Phys. Rev. A **79**, 043810 (2009).

[75] Y. He *et al.*, Dynamically controlled resonance fluorescence spectra from a doubly dressed single InGaAs quantum dot, Phys. Rev. Lett **114**, 097402 (2015).

[76] G. S. Agarwal, Anisotropic vacuum-induced interference in decay channels, Phys. Rev. Lett. **84**, 5500 (2000).

[77] Y. Yang, J. Xu, H. Chen, and S. Zhu, Quantum interference enhancement with left-handed materials, Phys. Rev. Lett. **100**, 043601 (2008).

[78] V. Yannopapas, E. Paspalakis, and N. V. Vitanov, Plasmon-induced enhancement of quantum interference near metallic nanostructures, Phys. Rev. Lett. **103**, 063602 (2009).

[79] P. K. Jha, X. Ni, C. Wu, Y. Wang, and X. Zhang, Metasurface-enabled remote quantum interference, Phys. Rev. Lett. **115**, 025501 (2015).

[80] S. Hughes and G. S. Agarwal, Anisotropy-induced quantum interference and population trapping between orthogonal quantum dot exciton states in semiconductor cavity systems, Phys. Rev. Lett. **118**, 063601 (2017).

[81] V. Karanikolas and E. Paspalakis, Plasmon-induced quantum interference near carbon nanostructures, J. Phys. Chem. C **122**, 14788 (2018).